Transient Absorption Studies and Numerical Modeling of Iodine Photoreduction by Nanocrystalline TiO_2 Films

Alex N. M. Green,[†] Rosemary E. Chandler,[‡] Saif A. Haque,[†] Jenny Nelson,*[,‡] and James R. Durrant*[,†]

Centre for Electronic Materials and Devices, Department of Chemistry, Imperial College of Science, Technology and Medicine, London, SW7 2AZ, United Kingdom, and Centre for Electronic Materials and Devices, Department of Physics, Imperial College of Science, Technology and Medicine, London, SW7 2BZ, United Kingdom

Received: June 15, 2004; In Final Form: October 15, 2004

We have used transient absorption spectroscopy to study the reaction between photogenerated electrons in a dye-free nanocrystalline titanium dioxide film and an iodine/iodide redox couple. Recombination kinetics was measured by recording the transient optical signal following band gap excitation by a UV laser pulse. In the presence of a methanol hole scavenger in the electrolyte, a long-lived (0.1−1 s) red/infrared absorbance is observed and assigned to photogenerated electrons forming Ti^{3+} species. In the presence of iodine and excess iodide in the electrolyte, the signal decays on a millisecond−microsecond time scale, assigned to reduction of the redox couple by photogenerated electrons in the TiO_2. The electron lifetime decreases inversely with increasing iodine concentration, indicating that the back reaction is first order in $[I_2]$. No evidence for I_2^- is observed, indicating that the reaction mechanism does not involve the formation of I_2^- as an intermediate. The shape of the kinetics evolves from monoexponential at low $[I_2]$ to stretched-exponential as $[I_2]$ increases. A Monte Carlo continuous-time random walk model is implemented to simulate the kinetics and its $[I_2]$ dependence and used to address the order of the recombination reaction with respect to electron density, *n*. The model incorporates the diffusion of oxidized species from the electrolyte toward the TiO_2 surface as well as electron trapping and transport in the TiO_2. In the limit of low $[I_2]$, the monoexponential kinetics is explained by the recombination reaction being rate limited by the diffusion of the oxidized species in the electrolyte. The stretched-exponential behavior at high $[I_2]$ can be explained by the reaction being rate limited by the transport of electrons through a distribution of trap states toward reactive sites at the TiO_2−electrolyte interface, similar to the mechanism proposed previously for the kinetics of electron−dye cation recombination. Such trap-limited recombination can also explain the superlinear dependence of electron recombination rate on electron density, which has been reported elsewhere, without the need for a reaction mechanism that is second order in *n*. In contrast, a second-order reaction mechanism in a trap-free medium cannot explain the observed kinetics, although a second-order mechanism incorporating electron trapping cannot be conclusively ruled out by the data. We propose that the most likely reaction scheme, that is first order in both $[I_2]$ and *n*, is the dissociative reduction of I_2 onto the metal oxide surface, followed by a second electron reduction of the resulting adsorbed iodine radical, and that empirical second-order behavior of the electron lifetime is most likely explained by electron trapping rather than by a second-order recombination mechanism.

Introduction

Dye-sensitized photoelectrochemical solar cells are attracting widespread academic and commercial interest due to their potential for low cost solar energy conversion. Such devices are based upon the sensitization of mesoporous, nanocrystalline metal oxide films by molecular dyes. Charge separation in such devices is achieved by ultrafast electron injection from the photoexcited sensitizer dye into the conduction bands of the semiconductor.[1,2] This ultrafast charge separation is followed by regeneration of the dye ground state by a redox electrolyte interpenetrated into the film pores, typically iodine/iodide redox couple in an organic solvent. Following charge separation, electrons must be transported through the nanocrystalline electrode, and oxidized species in the electrolyte through the pores of the electrode, to reach an external circuit. For high device efficiency, these carrier collection processes must compete favorably with interfacial recombination processes. However, the large interfacial area enhances the probability of recombination.[1,2] Minimization of such interfacial recombination processes is critical to device function.

Two recombination pathways exist at the interface between the sensitized metal-oxide and the redox active electrolyte. One is the re-reduction of the dye cation by photoinjected electrons, and the other is the recombination of photoinjected electrons directly with oxidized species in the electrolyte, which we will call the "back reaction". In the commonly used iodine/iodide redox couple, this second recombination reaction can be summarized as

$$2e^- + I_3^- \rightarrow 3I^- \quad (1)$$

* Corresponding authors. E-mail: j.durrant@imperial.ac.uk, jenny.nelson@imperial.ac.uk.
[†] Department of Chemistry.
[‡] Department of Physics.

10.1021/jp047414p CCC: $30.25
Published on Web 12/15/2004

Unlike the dye cation re-reduction, the back reaction can also occur in the dark and is responsible for the dark current of the dye-sensitized solar cell.

The first pathway, dye cation re-reduction, has been studied extensively.[3] In the presence of sufficient concentrations of iodide and sufficiently conductive electrolytes, this recombination pathway can normally be neglected due to the rapid rate of reduction of the oxidized dye molecules by iodide,[4,5] although this pathway may become significant at high device operating voltages and with alternative pseudohalogen redox couples[6] or low conductivity electrolytes.[5] Frequency resolved photovoltage studies show little dependence of electron lifetime on the presence of the dye, indicating that the back reaction dominates.[7] Other evidence for the functional importance of the back reaction comes from the decrease in open-circuit voltage,[8,9] the loss in photocurrent quantum efficiency,[10] and the increase in dark current[8,9] with increasing iodine concentration. The back reaction also appears critical in quasi-solid-state devices, where increasing iodine concentration leads to reduced electron lifetime in ionic liquid electrolytes[11] and to reduced open-circuit voltage in polyiodide electrolytes.[12] The dark current is also affected by other components of the redox electrolyte including pyridine,[8] lithium cations,[9] type of solvent used,[13] and deoxygenation.[13]

As the second pathway appears to dominate both open-circuit voltage and dark current of the dye-sensitized solar cell (DSSC), then it is clearly of key importance to understand the factors determining the recombination rate and the specific reaction scheme controlling eq 1. The reaction stoichiometry given by eq 1 indicates that the reaction is likely to proceed via several intermediate steps, and several distinct kinetic models have been proposed which differ in the order of the reaction with respect to iodine concentration, $[I_2]$, and electron density, n. A number of experimental studies have addressed the dynamics of this back reaction, particularly using frequency domain techniques, to study the reaction at quasi-steady-state conditions. Techniques used include intensity modulated photovoltage spectroscopy,[7,14−17] intensity modulated absorbance,[7,17] transient charge extraction,[18] and steady-state current−voltage characteristics as a function of intensity and $[I_2]$.[8,9] Several of these studies concluded that the recombination rate is approximately second order with respect to n,[8,14,15,18] and some further studies report second-order behavior with respect to $[I_2]$.[8] To explain the apparent second-order behavior, the following scheme has been proposed:[15]

SCHEME 1

$$I_3^- \leftrightarrows I_2 + I^- \quad (2)$$

$$I_2 + e_{cb}^- \leftrightarrows I_2^{-\bullet} \quad (3)$$

$$2I_2^{-\bullet} \rightarrow I_3^- + I^- \quad \text{(Scheme 1a)} \quad (4a)$$

$$I_2^{-\bullet} + e_{cb}^- \rightarrow 2I^- \quad \text{(Scheme 1b)} \quad (4b)$$

The net reaction is second order in n provided that reaction 3 is in equilibrium, as proposed by Huang et al.[8] It will be second or first order with respect to $[I_2]$ depending on which of reactions 4a and 4b dominates. If, on the other hand, reaction 3 is instead the rate-determining step, then the scheme is first order in n and effectively first order in $[I_2]$. Kopidakis and co-workers recently concluded that reaction 3 should be rate determining from a study of transport and recombination dynamics that suggested effective first-order dependence on both $[I_2]$ and n.[16] Peter[20] has also proposed that Scheme 1b is followed but with reaction 3 as the rate-determining step, to yield a net first-order dependence on $[I_2]$.

An alternative first-order mechanism was proposed by Liu et al. to explain apparent first-order behavior with respect to both iodine and electron density from studies of current−voltage characteristics.[9] The scheme involves dissociative adsorption of I_2 onto the metal oxide surface (step 5 below) followed by rapid[19] scavenging of conduction band electrons by the adsorbed iodine radicals:

SCHEME 2

$$I_3^- \leftrightarrows I_2 + I^- \quad (2)$$

$$I_2 + e^- \rightarrow I_{ads} + I^- \quad (5)$$

$$I_{ads} + e^- \rightarrow I^- \quad (6)$$

This scheme is analogous to the reduction of iodine at the platinum counter electrode in a DSSC when generating a photocurrent.

Identifying the correct reaction scheme and factors determining back-reaction kinetics is critical for device optimization and for quantitative modeling of current−voltage characteristics. The arguments for using a model that is second order in electron density are based on the observation of empirical second-order behavior, typically through experimental observation of an electron lifetime that scales approximately inversely with the light intensity at open circuit.[20] This intensity-dependent electron lifetime is important to device function, as it counteracts the intensity dependence of the electron diffusion coefficient in the TiO_2 to lead to sustained good performance of dye-sensitized solar cells at low light levels.[20]

An alternative explanation for the empirical superlinear n dependence of the back-reaction rate that is still consistent with a first-order reaction scheme can be found by considering the effect of electron trapping on recombination. Extensive transient optical studies of the kinetics of the first mentioned recombination pathway, the re-reduction of the dye cation, have shown that the experimentally observed order of this one-electron reduction reaction with respect to n is greater than 1 and may be as great as 4.[21,22] This has been attributed to a mechanism where recombination is rate limited by electron diffusion through an approximately exponential distribution of trap energies before finding the dye cation. The final, interfacial electron transfer step is shown to be limiting only in the case of very slow interfacial electron transfer,[23,24] and in those cases the kinetics becomes first order. It was proposed by Nelson et al.[21] that if electron trapping is also the rate-limiting step in the back reaction to the redox couple, then this would lead to a superlinear dependence of recombination rate on n and could explain the observed kinetics without need for a second-order reaction scheme. The same conclusion was reached independently by Kopidakis and co-workers.[16]

Previous theoretical models of the back reaction proposed to date have generally assumed that the back reaction is the only recombination pathway. Most have described it as a quasi-first-order process,[25−27] and some as a second-order process[28] or as a Shockley−Read−Hall process based on semiconductor theory,[29] but the effect of trapping in a distribution of trap sites has not previously been considered.

In this paper, the transient optical technique is extended to the back reaction by exploiting the well-known red−infrared absorbance of conduction band electrons in the nanocrystalline TiO_2. Optical techniques have been used previously to monitor

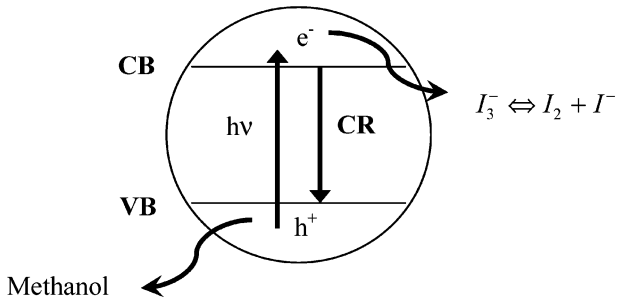

Figure 1. Schematic diagram showing the reaction scheme of the experiment. Pulsed band gap excitation of the nanocrystalline TiO_2, in the absence of sensitizer dyes, results in the generation of electron−hole pairs. A hole scavenger such as methanol is employed to scavenge photogenerated holes from the film, resulting in long-lived conduction band electrons. The reaction of these electrons with the iodine/iodide redox couple is then monitored by following the decay of the photoinduced absorption of the TiO_2 electrons. This technique allows us to probe the kinetics of the recombination reaction (eq 1) directly and investigate the possible formation of any transient intermediates.

electron dynamics in both frequency and time domain.[7,17,30,31] In the present work, pulsed band gap excitation of a nanocrystalline TiO_2 electrode in the presence of a hole scavenger results in long-lived conduction electrons, whose density may be probed directly by monitoring the decay in photoinduced absorption after the laser pulse. The principle is illustrated schematically in Figure 1. A dye-free system is used in order to focus exclusively on the back reaction of electrons with the I_2/I^- redox couple. In the limit of high $[I_2]$, we observe stretched exponential kinetics similar to those observed for trap-limited recombination, and in the limit of low $[I_2]$ the kinetics becomes monoexponential, apparently limited by the availability of I_2 species in the electrolyte. The advantage of the transient optical technique relative to techniques based on current or voltage dynamics is that the recombination is monitored directly, without need for conduction to an external circuit. We use a numerical model, implemented with Monte Carlo simulations, to show that the behavior can be explained by trap-limited electron diffusion alone, without the need for a second-order reaction scheme. Furthermore we show that second-order recombination *without* electron trapping cannot explain the observed behavior.

Experimental Details

All reagents were commercial grade and were obtained from Sigma-Aldrich or their subsidiaries unless otherwise stated.

Sample Preparation. Fluorine-doped tin oxide conducting glass (15 Ω/square, Hertford Glass) was placed in acetone and sonicated for 30 min, then washed thoroughly with deionized water and dried in the furnace at 450 °C. Nanocrystalline titanium dioxide colloids (∼15 nm) were prepared as described in previously published methods.[22,32,33] Films (4 μm thickness) were deposited using the doctor-blade technique on the conducting glass substrates. The resulting films consisted of TiO_2 particles approximately 15 nm in diameter and over 90% anatase as determined by Raman spectroscopy. The film density and Brunauer−Emmett−Teller (BET) analysis indicated a pore volume fraction of 50% and surface area of 100 m^2/g. The films were cut up into smaller electrodes with an active area of 1 cm^2 and stored under a dry atmosphere. Counter electrodes were then prepared by chemically depositing platinum from 0.05 M hexachloroplatanic acid in 2-propanol onto a second slide of conducting glass.

A "sandwich cell" was prepared by sealing together the TiO_2-coated electrode with the counter electrode using a transparent film of Surlyn 1472 polymer (DuPont Ltd.) at 110 °C. The electrolyte was introduced through holes drilled in the counter electrode, which were sealed immediately with microscope cover slides and additional strips of Surlyn to avoid leakage unless otherwise stated. The electrolyte consisted of 0.6 M tetrabutylammonium iodide, 0.1 M lithium iodide, 0.5 M 4-*tert*-butylpyridine, and 1−100 mM of iodine dissolved in an acetonitrile (HPLC grade, Fluka) and 10 vol % methanol (BDH Analar grade) solvent, both dried prior to use by 4 Å molecular sieves. Argon gas was bubbled through the electrolyte prior to the fabrication of sandwich cells in order to remove any oxygen. Sandwich cells were prepared with varying concentrations of iodine (1−100 mM) in order to study the dependence on iodine concentration of the back reaction. In addition, three control samples were also assembled. The first of these contained an electrolyte comprising degassed acetonitrile only, the second contained acetonitrile with 10% methanol as a hole scavenger, and the third sample contained an electrolyte containing a 0.1 M solution of $Fe[CN]_6^{4-}$ in acetonitrile as a hole scavenger.

Transient Absorption Spectroscopy. Recombination kinetics between electrons and holes in the TiO_2 and electrons and the iodine/iodide redox couple was monitored using microsecond−millisecond transient absorption spectroscopy.[22] Band gap excitation of the TiO_2 was achieved by using a PTI GL-3300 nitrogen laser as the excitation source (337 nm, 0.6 mJ cm^{-2}, 0.8 Hz, 600 ps pulse duration). A light guide was used to transmit the pulse to the sample. The probe light was provided by a 100 W tungsten lamp, with wavelength selection being achieved by monochromators before and after the sample. Changes in optical density induced by the excitation pulse were monitored with a silicon photodiode, home-built amplification/filtering system and digitized by a Tektronix TDS220 digital storage oscilloscope.

Experimental Results

Our experimental protocol is based upon band gap excitation of the nanocrystalline TiO_2 film, resulting in the generation of conduction band electrons and valence band holes. The holes are then rapidly scavenged in the presence of a high concentration of hole scavenger, allowing us to address the reaction of primary interest in this study, namely, the reaction of conduction band electrons with an I_2/I^- electrolyte. We have employed this experimental approach elsewhere to study the reaction of photogenerated TiO_2 electrons with molecular oxygen.[34]

We first consider the function of the hole scavengers employed in this study. Two scavengers were employed: methanol and $Fe(CN)_6^{4-}$, both of which are known to be readily oxidized by TiO_2 valence band holes.[33]

Figure 2 shows transient absorption spectra obtained at a time delay of 25 μs for the nanocrystalline TiO_2 in the absence (a) and presence (b) of methanol. The corresponding transient kinetics, observed at a probe wavelength of 800 nm, is shown in Figure 3. In the absence of methanol, a broad absorption increase is observed throughout the visible/near-infrared, consistent with the formation of electron−hole pairs within the TiO_2 film.[33] A rapid decay of this photoinduced absorption is observed (half-life < 10 μs), which we attribute to prompt recombination of photogenerated electrons and holes within the TiO_2 film, consistent with previous observations.[34−36]

The addition of 10% methanol to the degassed acetonitrile results in clear changes in both the photoinduced absorption spectrum (Figure 2) and the decay dynamics (Figure 3). The transient spectrum increases in amplitude to toward the near-infrared, consistent with its assignment to TiO_2 conduction band

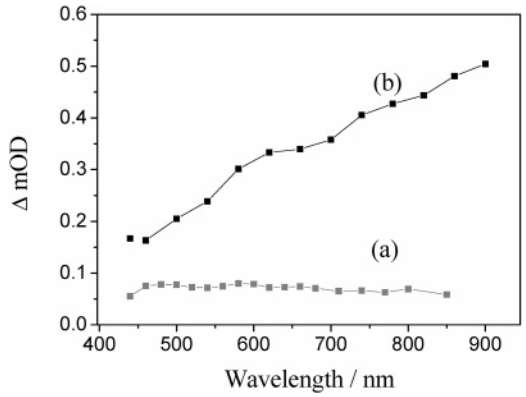

Figure 2. (a) Transient absorption difference spectra obtained following band gap excitation of nanocrystalline TiO_2 films in degassed acetonitrile in (a) the absence and (b) the presence of 10 vol % of methanol. Spectra were collected at a time delay of 25 μs.

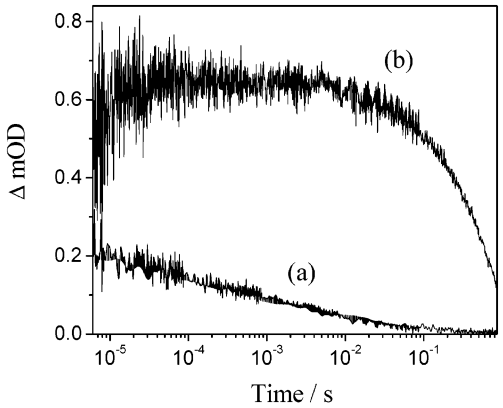

Figure 3. Transient absorption kinetics obtained following band gap excitation of nanocrystalline TiO_2 films in degassed acetonitrile in (a) the absence and (b) the presence of 10% methanol by volume. Kinetics were collected at a probe wavelength of 800 nm.

electrons in the absence of valence band holes.[33] The decay dynamics of this photoinduced absorption is dramatically retarded in the presence of methanol, with a half time of ~0.5 s for decay of the photoinduced absorption. Note also that the kinetics, which is highly nonexponential in the absence of methanol, spanning time scales from 10^{-6} to 0.1 s, becomes approximately monoexponential when methanol is added. It can be concluded that the methanol scavenges photoinduced TiO_2 holes on a time scale faster than the experimental resolution for the data reported here (<1 μs). This scavenging effectively competes with electron−hole recombination within the film, leading to the generation of long-lived photogenerated conduction band electrons. Similar long lifetimes for electrons in the absence of redox couple have been reported previously.[30]

The hole scavenging function shown in Figures 2 and 3 was found to not be specific to the hole scavenger employed. Indistinguishable lifetimes of long-lived TiO_2 conduction band electrons were obtained for the hole scavengers methanol and $Fe(CN)_6^{4-}$, as shown in Figure 4, although the yield of long-lived electrons was found to be higher using methanol as a hole scavenger. We note that in both cases the hole scavenging function will generate oxidized species thermodynamically capable of being reduced by TiO_2 conduction band electrons. It is however apparent from the data shown in Figure 4 that any such dynamics is slow (half time ≥ 0.5 s) and will therefore not interfere with our studies of the iodine reduction detailed below.

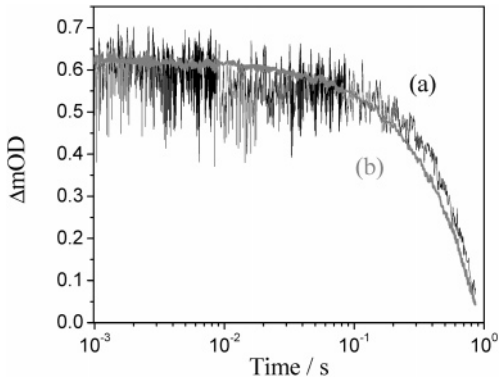

Figure 4. Transient absorption kinetics obtained following band gap excitation of nanocrystalline TiO_2 films in degassed acetonitrile in the presence of two different hole scavengers: (a) 0.1 M $Fe(CN)_6^{4-}$ and (b) 10% methanol. Kinetics were collected at a probe wavelength of 800 nm.

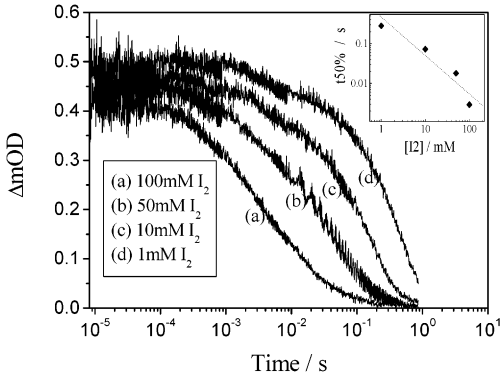

Figure 5. Transient absorption kinetics obtained following band gap excitation (337 nm) of nanocrystalline TiO_2 films in degassed acetonitrile in the presence of 10% methanol, 0.7 M I^-, and concentrations of added iodine ranging from 1 to 100 mM as indicated. Kinetics were collected at a probe wavelength of 800 nm. The inset shows the half-life of the kinetic curves as a function of iodine concentration, in comparison with first-order behavior (dotted line).

We now consider the transient absorption dynamics in the presence of the I_2/I^- redox couple, as shown in Figure 5. Data are shown as a function of iodine concentration, with the iodide concentration maintained at 0.7 M. As the iodine concentration is increased, the decay dynamics of the photoinduced absorption accelerates, consistent with faster recombination of conduction band electrons with oxidized species in the redox couple. Increasing the iodide concentration from 1 to 100 mM results in an acceleration of the decay half time from 200 to 3 ms, indicative, as we discuss below, of a first-order dependence of the electron transfer reaction upon iodine concentration. The I_2/I^- redox couple exhibited negligible hole scavenging activity, with control data collected in the absence of hole scavenger showing only a fast (<10 μs) decay indistinguishable from that shown in Figure 3, trace a, and assigned to electron−hole recombination within the TiO_2 nanoparticles.

The transient absorption spectrum at 25 μs was found to be unaffected by the addition of the redox couple, confirming the assignment of the transient signal to TiO_2 conduction electrons. We note that no evidence was observed for the formation of long-lived $I_2^{-\bullet}$ transients. This contrasts with our previous transient optical studies of I_2/I^- electrolyte function in contact with dye-sensitized TiO_2 electrodes, where dye cation reduction by iodide results in the formation of a long-lived (half time of ~0.5 s) transient signal with a transient spectrum characteristic of I_2^- radicals.[4] The absence of any long-lived I_2^- transients

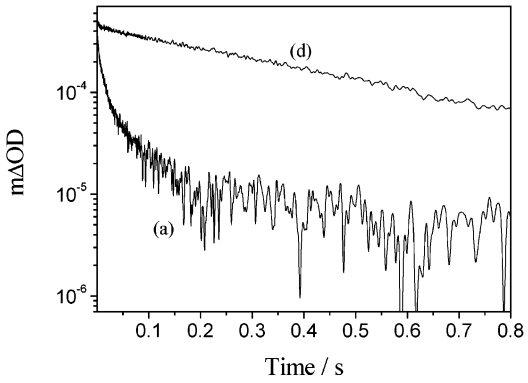

Figure 6. Transient data from Figure 5 (traces a and d, corresponding to 100 and 1 mM I_2, respectively) replotted on log−linear (rather than linear−log) axes, illustrating the transition from a slow, monoexponential decay at 1 mM I_2 to faster, more dispersive dynamics at high iodine concentrations.

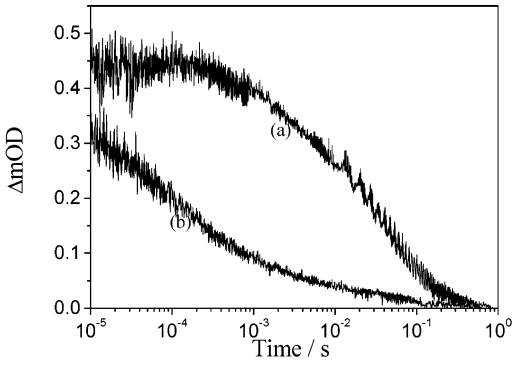

Figure 7. Transient absorption kinetics obtained following band gap excitation (337 nm) of nanocrystalline TiO_2 films in degassed acetonitrile with 10% methanol, 50 mM I_2 M, and the presence (a) or absence (b) of 0.7 M I^-. Kinetics were collected at a probe wavelength of 800 nm.

has important implications for the reaction mechanism, as we discuss below.

It is apparent from Figure 5 that increasing the iodine concentration has a strong impact not only on the half time of the decay dynamics but also on the temporal shape of the dynamics. As the iodine concentration increases, the dynamics becomes increasingly dispersive. This is shown more clearly in Figure 6, which shows a log−linear (rather than linear−log) plot of the decay dynamics with 1 and 100 mM iodine. From this plot, it is apparent that at 1 mM iodine the decay of photoinjected electrons is approximately monoexponential. However, at the higher iodine concentration (100 mM) the kinetics deviates strongly from monoexponential behavior. Such data show a better fit to a stretched-exponential function, $\Delta OD \propto e^{-(t/\tau)^{\alpha}}$, with a dispersion parameter α in the range 0.5−0.7. A similar transition from slow, monoexponential recombination dynamics to faster, dispersive dynamics has been reported previously for electron−dye cation recombination dynamics as a function of sensitizer dye design.[23,24,37] In the present case, it can be attributed to a transition between charge recombination dynamics rate limited by dispersive electron transport within the TiO_2 nanoparticles, in the limit of high iodine concentration, to recombination dynamics rate limited by the availability of oxidized species at the interface in the limit of low iodine concentration. This is discussed in more detail below.

In the presence of excess iodide, as is the case for the data shown in Figure 5 and for functioning dye-sensitized solar cells, iodine in the electrolyte is largely present in the form of triiodide, I_3^-, through reaction 2 above ($I_3^- \Leftrightarrow I_2 + I^-$). The equilibrium constant for this reaction in acetonitrile has previously been estimated to be 10^{-7} mol dm^{-3},[38] indicating that for all electrolyte compositions employed in Figure 5, $[I_2] \ll [I_3^-]$. To evaluate the relative importance of I_2 and I_3^- species in the back reaction, data were collected with a fixed concentration of iodine (50 mM) in the presence and absence of excess (0.7 M) iodide, as shown in Figure 7. It is apparent that in the absence of iodide, the decay dynamics accelerates by around 2 orders of magnitude (half time of ~10 ms and 80 μs in the presence and absence of iodide, respectively) and furthermore becomes more dispersive. The acceleration of the dynamics in the absence of iodide clearly demonstrates a faster reaction of TiO_2 electrons with iodine alone compared to the equilibrium combination of I_2 and I_3^-. This observation is consistent with previous suggestions[16] that iodine is the main electron acceptor in the back reaction to the redox couple, which may be explained partly by the unfavorable electrostatic interactions expected between conduction band electrons and I_3^- species.

Modeling. To simulate the back-reaction kinetics and attempt to distinguish between different reaction mechanisms, we use a version of the continuous-time random-walk model (CTRW) as proposed by Nelson.[21,39] In the model, electrons execute a random walk independently on a cubic lattice representing part of the TiO_2 nanocrystalline film, taking each step after an interval defined by the activation energy of the site currently occupied. The site energies may be identical, representing a trap-free medium, or they may be distributed according to some density of states function. The CTRW represents a multiple trapping mechanism where electrons are thermally activated out of and captured into trap states below the TiO_2 conduction band edge. In the simplest version, recombination occurs when electrons meet a reactive site or "target". Such a model was used previously[21,39] to show that multiple trapping and detrapping dominate the recombination kinetics of electrons with the dye cation. In that case, the targets were photo-oxidized dye molecules, while in the current case the targets represent oxidized species in the electrolyte.

The details of the CTRW model as applied to nanocrystalline TiO_2 are described elsewhere.[21,39] For the present purpose, the model is modified so that the targets for the recombination of mobile electrons are oxidized species in the electrolyte, rather than dye cations, and the population of photogenerated electrons, rather than dye cations, is monitored to compare with the measured transient absorbance. The rules for recombination depend on whether the reaction is first or second order in electron density and are defined below. We consider the cases of first-order recombination in the presence of traps, second-order recombination in the presence of traps, and second-order recombination in a trap-free medium. In all cases, the recombination reaction is first order with respect to $[I_2]$ as this is clearly shown by the experimental data. To simulate the behavior in dilute electrolytes, the model is modified, as described below, to regenerate the target population during simulation, in order to simulate the diffusion of oxidized species from the bulk of the electrolyte toward the TiO_2 film surface.

The simulation volume is a regular cubic lattice of size s^3 lattice units ($s = 64$), into which N_0 electrons and H_0 targets are generated at random locations at time $t = 0$. The lattice constant a_{latt} represents the distance between neighboring Ti atoms (0.4 nm in anatase[40]), and periodic boundary conditions are applied in all directions. The energies, E, of the sites are distributed according to the exponential distribution function

$$g(E) = \frac{1}{kT_0}\exp(-(E_c - E)/kT_0) \quad (7)$$

where k is Boltzmann's constant, E_c is the conduction band edge energy, and T_0 is the characteristic temperature of the distribution corresponding to a dispersion parameter, α.

$$\alpha = T/T_0 \quad (8)$$

Here T is the ambient temperature (300 K). To simulate thermally activated diffusion, each electron is moved to one of its unoccupied neighboring sites at random after a time

$$t = -\frac{\ln \gamma}{\nu_0}\exp((E_c - E)/kT) \quad (9)$$

where E is the energy of the site currently occupied, ν_0 the attempt to jump frequency, and γ a random number between 0 and 1. To simulate trap filling, multiple occupancy of sites is forbidden. The simulation volume represents part of the nanocrystalline film, of volume equivalent to a few nanoparticles, plus the fraction, F_{rec}, of the electrolyte volume that is close enough to the TiO_2 film surface to take part in the back reaction. Specific nanoparticle geometries are not applied, since it was shown previously[21] that for a deep enough distribution of trap states, recombination kinetics is insensitive to the shape of the simulation volume or the spatial distribution of traps, apart from through a time scale factor.

For each simulation, the initial population of targets, H_0, is calculated from the experimental iodine concentration. The targets represent the reactive species in the back reaction, i.e., I_2 molecules and I_3^- ions which are capable of dissociating quickly via reaction 2. It has been argued above and elsewhere[18] that I_2 molecules are the reactive species, and I_2 generation is clearly the first step in all the reaction schemes proposed above. Although we do not know the extent to which I_3^- ions act as targets for the back reaction, it is clear that, at the high experimental iodide concentrations used, the initial target population will be proportional to the initial $[I_2]$ concentration. The constant of proportionality is absorbed into the factor representing the active electrolyte volume, so that

$$H_0 = F_{rec}\rho_{I_2}(a_{latt}s)^3 \quad (10)$$

where ρ_{I_2} is the volume concentration of iodine added to the bulk electrolyte. The initial population of photogenerated electrons added to the simulation volume at $t = 0$, N_0, is estimated as 14 in a simulation volume of side $s = 64$ from the experimental change in optical density at 800 nm of 4.4×10^{-4} using an extinction coefficient of 800 M^{-1} cm^{-1} for conduction electrons in TiO_2 at 800 nm.[41] This is consistent with the estimated laser power of 600 μJ cm^{-2} $pulse^{-1}$.

The back reaction is simulated by allowing the N_0 photogenerated electrons to perform a random walk on the lattice and recording the times at which electrons meet and recombine with target species. We have simulated both first-order and second-order recombination, with respect to n. In the first-order model, recombination occurs as soon as an electron walks onto a site occupied by a target, and both electron and target are removed from the lattice. In the second-order model, when an electron meets an unoccupied target, it remains with the target for a certain residence time, t_{res}. If a second electron arrives during this residence time, then recombination occurs and the target and both electrons are removed from the lattice. Otherwise, the first electron leaves the target and continues its walk. Short residence times lead to second-order kinetic behavior. This is easily seen by simulating the process on a trap-free lattice, where all lattice sites have the same energy, in which case the electron population decays like $1/t$ at long times. Long residence times lead to quasi-first-order behavior. Physically the second-order model represents Scheme 1b where reaction 3 is in equilibrium, while the first-order model represents either Scheme 2 or Scheme 1b where step 3 is rate determining. In each case, as the electrons recombine with the targets, more targets are generated into the lattice as described below. The simulation ends when there are no more electrons left.

To model kinetics in low $[I_2]$ conditions, we incorporate a mechanism of target regeneration to simulate the replenishment of targets in the reactive volume by diffusion of I_3^- from the bulk of the electrolyte. We assume a "target generation rate" that depends on the deviation from the equilibrium target concentration in the system:

$$\frac{dH}{dt} = k_H(H_0 - H) \quad (11)$$

where H is the current number of targets, k_H is a constant proportional to the target diffusion coefficient, and t is time. k_H is treated as a fitting parameter, and the time scale is defined by the attempt-to-jump frequency ν_0. Equation 11 is consistent with a diffusive flux density of targets moving into the interfacial region and implies that target generation will be fastest when the target depletion $(H_0 - H)$ is a large fraction of H_0. Target generation is implemented by calculating the mean number of targets to be added, $\Delta H(t)$, at the end of each step in the simulation where t is the step length, given by

$$\Delta H(t) = H_0(1 - e^{-k_H t}) \quad (12)$$

by integration of eq 11, and randomizing the value to allow rare events. The time intervals are short enough that ΔH is normally 0 or 1.

In cases where targets are completely depleted, computation is speeded up by halting the simulation when $H = 0$ and advancing the time to the next target generation event. "Halting" implies that the carrier population reaches its equilibrium configuration before the halt is applied. This assumption was verified by test simulations, in agreement with previous studies[42,43] which show that equilibration of carrier hopping in disordered lattices does indeed occur quickly.

The relevant parameters for the simulation are α, the room-temperature dispersion parameter for the density of states, ν_0, the attempt-to-jump frequency which defines the time scale, F_{rec}, which defines the fraction of iodine molecules which take part in the back reaction, and k_H, the tri-iodide diffusion coefficient. For both first-order and second-order models, our methodology was as follows. First the value of α was found by fitting the highest $[I_2]$ kinetic trace, assuming that ion diffusion was unimportant in this limit. The value of k_H was estimated from the time constant of the lowest $[I_2]$ trace. Then the simulations at the four different experimental concentrations were repeated for a given value of F_{rec} until the best fit was found, using ν_0 as a free parameter. The main effect of F_{rec} is to control the dependence of the electron lifetime on $[I_2]$. In the second-order model, the residence time is chosen to be short compared to the electron wait time (calculated from eq 9).

Figure 8 shows the first-order model fitted to the experimental data from Figure 5. The parameters used are listed in Table 1 below. The simulations predict stretched-exponential kinetics at high $[I_2]$ values, tending to monoexponential at low $[I_2]$. This

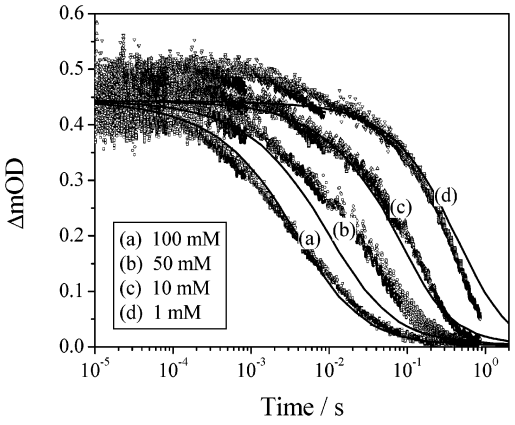

Figure 8. First-order target generation model fitted to transient absorption spectroscopy. Symbols represent experimental data; full lines represent the simulation results.

TABLE 1: Free Parameters Used to Fit the First-Order Model to the Experimental Data

parameter	value	parameter	value
a	0.72	F_{rec}	0.05
$1/\nu_0$	5.5×10^{-8}	k_H	$4.5 \times 10^3\ s^{-1}$

is consistent with back-reaction kinetics at low iodine concentrations that is rate limited by the diffusion of the redox species from the bulk electrolyte toward the TiO_2 surface, while at high iodine concentrations the kinetics is rate-limited by electron diffusion in the TiO_2, with diffusion of the redox species playing a minor role.

The value of α used to fit the data is larger than values reported previously for the density of states in nanocrystalline TiO_2.[15,22,39] Although a smaller value of α (down to 0.5) could be used to fit the highest $[I_2]$ curve equally well, the shape of the lower $[I_2]$ curves would not be reproduced well using any values of F_{rec} or k_H. Similar arguments apply to the second-order model. The reason for the larger value of α is not known, but it is conceivable that the density of states involved in electron recombination to the electrolyte may be different from that involved with recombination to the dye cation. For instance, if recombination could occur from some deep traps directly to the electrolyte without detrapping, the effective density of trap states determining recombination kinetics would appear shallower.

The best-fit value of $F_{rec} = 0.05$ corresponds to a reactive volume at least 0.125 nm thick over the surface of a spherical nanoparticle of diameter 15 nm, assuming that all I_2 molecules and I_3^- ions act as targets, or to a larger reactive volume if I_3^- ions are less effective electron scavengers than I_2. A much larger value of F_{rec} would predict an even stronger sensitivity of half-life to $[I_2]$ than that observed experimentally and would not be able to fit the data. The diffusion rate of $k_H = 4.5 \times 10^3\ s^{-1}$ can be converted to a diffusion coefficient as shown in the Appendix. If the targets diffuse over the thickness of the film of 4 μm (i.e., if the gradient in $[I_2]$ extends over the film thickness), then the corresponding iodine diffusion coefficient is $D = 7.3 \times 10^{-4}\ cm^2\ s^{-1}$. The measured value of the iodine diffusion coefficient, $D = 10^{-6}\ cm^2\ s^{-1}$,[44] corresponds to iodine diffusion over a distance of approximately 10 nanoparticle diameters.

Figure 9 shows the results of simulations using the second-order recombination model. First we consider the kinetics resulting from second-order recombination in a trap-free medium (i.e., no disorder in the site energies on the simulation lattice), as represented by the filled circles in Figure 9. It is clear that

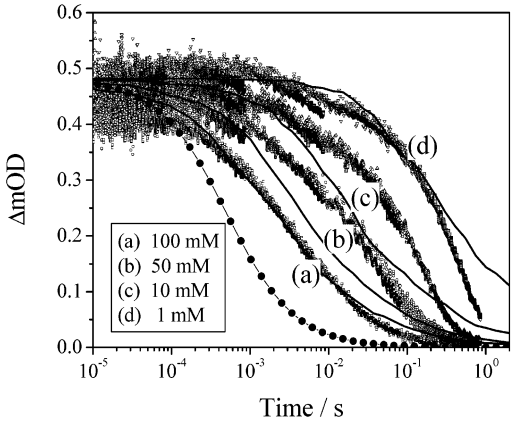

Figure 9. Second-order target generation model fitted to transient absorption spectroscopy data. Symbols represent experimental data; full lines represent the simulation results. The filled squares represent the result for a second-order recombination model in the absence of traps and should be compared with trace a.

TABLE 2: Free Parameters Used to Fit the Second-Order Model to the Experimental Data

parameter	value	parameter	value
a	0.7	k_H	$4.2 \times 10^4\ s^{-1}$
$1/\nu_0$	1.2×10^{-9} s	t_{res}	1.2×10^{-6} s
F_{rec}	1		

the shape of the kinetic curve is very different from the experimental kinetics in the limit of high $[I_2]$, and this model can therefore be ruled out. Next we consider second-order recombination in a medium containing an exponential distribution of traps. In this case, a reasonable fit could be found to the kinetics for the highest value of $[I_2]$, and the range of the kinetics between the limits of the highest and lowest $[I_2]$ values could also be reproduced, for a large enough value of F_{rec} and small enough value of the residence time. The best fit of the second-order model to the data is presented in Figure 9, and the corresponding parameter values are given in Table 2. However, the recombination kinetics at intermediate values of $[I_2]$ is not reproduced correctly and the simulated tail of the kinetic curve is too long. Note that the additional unknown of the residence time makes it impossible to pin down the values of the other parameters as closely as in the first-order case. However, the distribution of kinetic curves was not improved by any other parameter combinations tried. Overall, the fit obtained with the second-order model with trap states was thus less satisfactory than with the first-order model. However it cannot be definitively ruled out on the basis of the data presented here.

Discussion

First we comment on the order of the back reaction with respect to $[I_2]$. It was proposed by Huang et al., on the basis of the $[I_2]$ and intensity dependence of the open-circuit voltage of dye-sensitized solar cells, that the back reaction is second order with respect to $[I_2]$.[8] In contrast, Liu et al. concluded from similar measurements that the reaction was first order.[9] The data presented in Figure 5 clearly show that the half-life of the photogenerated electrons is approximately first order with respect to $[I_2]$, in agreement with Liu et al. This behavior is consistent both with reaction Scheme 1b where step 4b is fast compared to step 4a and with reaction Scheme 2.

Now we address the order of the back reaction with respect to electron density, n. The proposal that the kinetics of the back reaction is controlled solely by a second-order reaction scheme such as Scheme 1a or 1b[8,15,18] can be ruled out definitively by

the shape of the kinetic curves, as shown by the comparison of the trap-free simulation result with the experimental curves in Figure 9.

In contrast, the first-order model, Scheme 2, with an exponential distribution of trap states, as shown in Figure 8, succeeds in fitting the observed kinetic curves and their $[I_2]$ dependence with reasonable values of the fitting parameters. This indicates that, provided that electron trapping is incorporated, a first-order scheme for the interfacial electron transfer step is plausible and that electron trapping alone is sufficient to explain the superlinear dependence of the back-reaction rate on electron density. This explanation was proposed earlier[21,45] but without firm experimental evidence. It is consistent with the conclusion recently reached by Kopidakis et al., by consideration of the correlation between electron transport dynamics and back-reaction dynamics for electrodes in different chemical environments, that the back reaction is dominated by electron transport in the metal oxide and not by interfacial processes.[16] It is also consistent with the recent observation of a superlinear reaction order using an organic hole transporting molecule, MeOTAD, which is expected to undergo first-order recombination with the electron, as the redox species.[46] Moreover, in liquid electrolyte cells, a one-electron redox couple based on Co(II)/Co(III) has been shown to be almost as effective as the I_2/I^- redox couple,[47,48] disputing the notion that a multistep scheme is essential for good performance.

A second-order reaction scheme in the presence of traps is harder to rule out. Treating all parameters as free, the best fit obtained is shown in Figure 9. It is clear from this that the second-order mechanism again cannot reproduce the long time behavior of the kinetic curves or the detailed $[I_2]$ dependence of the kinetics, but the comparison of kinetic shape is better than in the trap-free case. To definitively rule out a second-order reaction with respect to n, it would be necessary to repeat the study with a redox couple known to undergo a first-order reaction with the electron and/or to study the transient optical kinetics as a function of externally injected electron density.

Further evidence against Schemes 1a and 1b comes from the lack of evidence for long-lived I_2^- species in our optical data. Previous studies have demonstrated the formation of I_2^- species as a result of the regeneration reaction in dye-sensitized TiO_2 films. These I_2^- species exhibited slow (0.2−0.5 s) decay kinetics, which was independent of the electrical bias applied to the TiO_2 film and therefore independent of electron density n. This latter observation indicates that the decay of these I_2^- species is dominated by the dismutation reaction 4a rather than the interfacial recombination reaction 4b. Integral to both Schemes 1a and 1b is the formation of I_2^- species, while no such species is generated in Scheme 2. Failure to observe any I_2^- species in the recombination studies reported here is clearly contrary to both Schemes 1a and 1b and supportive of Scheme 2. The failure to observe I_2^- species also argues against the alternative reaction scheme leading to first-order dependence on $[I_2]$, Scheme 1 where reaction 3 is rate limiting, that was proposed by Kopidakis and co-workers[16] and Peter and co-workers.[20] We note that any such I_2^- species should be readily observable in our studies due to their expected long lifetime[4] relative to the recombination dynamics addressed in this paper. Therefore we conclude that the back reaction is first order in both $[I_2]$ and electron density; the preferred reaction scheme is that proposed by Liu et al.,[9] Scheme 2 above.

Implications for Solar Cell Function

The iodine/iodide redox couple has been almost exclusively used as the redox mediator in DSSCs. Several studies have reported attempts to replace this couple in DSSCs with alternatives, including Br_2/Br^-,[51] quinone/hydroquinone,[51] ferrocene/ferrocenium,[51] SCN_2/SCN^-,[6] $Co(dbbip)_2^{3+}/Co(dbbip)_2^{2+}$,[52] and organic hole conductors.[53] While the latter two mediators are attracting significant interest, the device efficiencies with all of these mediators remain low relative to those achievable with the iodine/iodide couple.

Several studies have suggested that the high efficiency of devices employing the iodine/iodide redox couple may be associated with the two-electron redox chemistry of this couple, and specifically with the iodide to tri-iodide reduction process being second order in electron density. As such, the low electron density in the nanocrystalline TiO_2 film results in slow interfacial recombination dynamics and thereby the long electron lifetimes critical to efficient charge carrier collection by the electrodes. In this context, the low efficiency of alternative redox couples can be attributed to their one-electron redox chemistry. However, the study we report here indicates that the iodide to tri-iodide reduction process on nanocrystalline TiO_2 electrodes is most likely to be first order in electron density. This first-order behavior can be rationalized in terms of a reaction scheme in which the process is rate limited by a one-electron reductive step (reaction 6 in Scheme 2 above). As such, the high efficiency of DSSCs employing this couple cannot be attributed to the two-electron nature of the overall redox couple reduction. Therefore the slow interfacial recombination dynamics for DSSCs employing this couple must originate from a slow rate constant for this reaction. This slow rate constant can be most simply attributed to a large activation barrier for iodine dissociation at the nanocrystalline electrode (reaction 6).[54] This slow kinetics is further enhanced by the low concentration of molecular iodine in the redox electrolyte, with the dominant I_3^- species expected to be electrostatically repelled from the electrode under device operating conditions.[49] In contrast, the activation barrier for iodine dissociation is greatly reduced on the platinized counter electrode,[15,50] allowing efficient regeneration of the redox couple on the counter electrode and ensuring the vectorial transport of oxidizing equivalents from the dye-sensitized electrode to the counter electrode as required for efficient device function.

Acknowledgment. The authors thank Richard Monkhouse for the excellent electronics support and the EPSRC for financial support.

Appendix: Calculating the Diffusion Coefficient

In the model, target regeneration is assumed to follow the form

$$\frac{dH}{dt} = k_H(H_0 - H)$$

where H_0 and H are the initial and current numbers of targets and k_H is a fitted target diffusion rate. This can be rewritten in terms of a target flux, J [targets cm^{-2} s^{-1}], through an area A [cm^2], as

$$JA = k_H(H_0 - H)$$

Assuming that the target flux is diffusion driven, J can be related to a diffusion coefficient as usual,

$$J = D\frac{d\rho}{dx^{x=d}}$$

where ρ is the volume density of targets and d is the thickness of the film. Assuming that the concentration gradient falls over a distance of d' (which may be less than d), J can be approximated as

$$J = \frac{D(H_0 - H)}{A\delta d'}$$

where δ is the thickness of the reactive volume at the TiO_2 surface. This yields the relationship between k_H and D:

$$D = k_H \delta d'$$

References and Notes

(1) Hagfeldt, A.; Gratzel, M. *Acc. Chem. Res.* **2000**, *33*, 269.
(2) Durrant, J. R.; Haque, S. A.; Palomares, E. *Coord. Chem. Rev.*, in press.
(3) Haque, S. A.; Tachibana, Y.; Klug, D. R.; Durrant, J. R. *J. Phys. Chem. B* **1998**, *102*, 1745.
(4) Montanari, I.; Nelson, J.; Durrant, J. R. *J. Phys. Chem. B* **2002**, *106*, 12203.
(5) Nogueira, A. F.; De Paoli, M. A.; Montanari, I.; Monkhouse, R.; Nelson, J.; Durrant, J. R. *J. Phys. Chem. B* **2001**, *105*, 7517.
(6) Oskam, G.; Bergeron, B. V.; Meyer, G. J.; Searson, P. C. *J. Phys. Chem. B* **2001**, *105*, 6867.
(7) Franco, G.; Gehring, J.; Peter, L. M.; Ponomarev, E. A.; Uhlendorf, I. *J. Phys. Chem. B* **1999**, *103*, 692.
(8) Huang, S. Y.; Schlichthorl, G.; Nozik, A. J.; Gratzel, M.; Frank, A. J. *J. Phys. Chem. B* **1997**, *101*, 2576.
(9) Liu, Y.; Hagfeldt, A.; Xiao, X. R.; Lindquist, S. E. *Sol. Energy Mater. Sol. Cells* **1998**, *55*, 267.
(10) Lindstrom, H.; Rensmo, H.; Sodergren, S.; Solbrand, A.; Lindquist, S. E. *J. Phys. Chem.* **1996**, *100*, 3084.
(11) Kubo, W.; Kambe, S.; Nakade, S.; Kitamura, T.; Hanabusa, K.; Wada, Y.; Yanagida, S. *J. Phys. Chem. B* **2003**, *107*, 4374.
(12) Matsuda, T.; Matsumoto, H. *Electrochemistry* **2002**, *70*, 446.
(13) Stanley, A.; Verity, B.; Matthews, D. *Sol. Energy Mater. Sol. Cells* **1998**, *52*, 141.
(14) Schlichthorl, G.; Huang, S. Y.; Sprague, J.; Frank, A. J. *J. Phys. Chem. B* **1997**, *101*, 8141.
(15) Fisher, A. C.; Peter, L. M.; Ponomarev, E. A.; Walker, A. B.; Wijayantha, K. G. U. *J. Phys. Chem. B* **2000**, *104*, 949.
(16) Kopidakis, N.; Benkstein, K. D.; van de Lagemaat, J.; Frank, A. J. *J. Phys. Chem. B* **2003**, *107*, 11307.
(17) Zhu, K.; Schiff, E. A.; Park, N. G.; van de Lagemaat, J.; Frank, A. J. *Appl. Phys. Lett.* **2002**, *80*, 685.
(18) Duffy, N. W.; Peter, L. M.; Rajapakse, R. M. G.; Wijayantha, K. G. U. *J. Phys. Chem. B* **2000**, *104*, 8916.
(19) Fitzmaurice, D. J.; Eschle, M.; Frei, H.; Moser, J. E. *J. Phys. Chem.* **1993**, *97*, 3806.
(20) Peter, L. M.; Wijayantha, K. G. U. *Electrochim. Acta* **2000**, *45*, 4543.
(21) Nelson, J.; Haque, S. A.; Klug, D. R.; Durrant, J. R. *Phys. Rev. B* **2001**, *6320*, art. no.-205321.
(22) Willis, R. L.; Olson, C.; O'Regan, B.; Lutz, T.; Nelson, J.; Durrant, J. R. *J. Phys. Chem. B* **2002**, *106*, 7605.
(23) Clifford, J. N.; Yahioglu, G.; Milgrom, L. R.; Durrant, J. R. *Chem. Commun*. **2002**, 1260.
(24) Clifford, J. N.; Palomares, E.; Nazeeruddin, M. K.; Gratzel, M.; Nelson, J.; Li, X.; Long, J.; Durrant, J. R. *J. Am. Chem. Soc.* **2003**, *126*, 5225.
(25) Ferber, J.; Stangl, R.; Luther, *J. Sol. Energy Mater. Sol. Cells* **1998**, *53*, 29.
(26) Ferber, J.; Luther, J. *J. Phys. Chem. B* **2001**, *105*, 4895.
(27) Usami, A. *Chem. Phys. Lett.* **1998**, *292*, 223.
(28) Kambili, A.; Walker, A. B.; Qiu, F. L.; Fisher, A. C.; Savin, A. D.; Peter, L. M. *Physica E* **2002**, *14*, 203.
(29) Usami, A.; Ozaki, H. *J. Phys. Chem. B* **2001**, *105*, 4577.
(30) Boschloo, G.; Hagfeldt, A. *Chem. Phys. Lett.* **2003**, *370*, 381.
(31) Hagfeldt, A.; Lindquist, S. E.; Gratzel, M. *Sol. Energy Mater. Sol. Cells* **1994**, *32*, 245.
(32) Barbe, C. J.; Arendse, F.; Comte, P.; Jirousek, M.; Lenzmann, F.; Shklover, V.; Gratzel, M. *J. Am. Ceram. Soc.* **1997**, *80*, 3157.
(33) Bahnemann, D., Henglein, A.; Lilie, J.; Spanhel, L. *J. Phys. Chem.* **1984**, *88*, 709.
(34) Li, X.; Green, A. N. M.; Haque, S. A.; Mills, A.; Durrant, J. R. *J. Photochem. Photobiol., A* **2004**, *162*, 253.
(35) Rabani, J.; Yamashita, K.; Ushida, K.; Stark, J.; Kira, A. *J. Phys. Chem. B* **1998**, *102*, 1689.
(36) Haque, S. A.; Nelson, J.; Durrant, J. R. Transient optical studies of nanocrystalline TiO_2: Dynamics of electron recombination with an iodine/iodide redox couple. In *Photovoltaics for the 21st Century*; Electrochemical Society: Washington, 2001.
(37) Hirata, N., Lagref, J. J.; Palomares, E. J.; Durrant, J. R.; Nazeeruddin, M. K.; Gratzel, M.; Di Censo, D. *Chem.—Eur. J.* **2004**, *10*, 595.
(38) Nelson, J. *Electroanal. Chem.* **1964**, *7*, 218.
(39) Nelson, J. *Phys. Rev. B* **1999**, *59*, 15374.
(40) Sanjines, R.; Tang, H.; Berger, H.; Gozzo, F.; Margaritondo, G.; Levy, F. *J. Appl. Phys.* **1994**, *75*, 2945.
(41) Kolle, U.; Moser, J. E.; Gratzel, M. *Inorg. Chem.* **1985**, *24*, 2253.
(42) Anta, J. A.; Nelson, J.; Quirke, N. *Phys. Rev. B* **2002**, *65* art. no.-125324.
(43) Bassler, H. *Phys. Status Solidi B* **1993**, *175*, 15.
(44) Kebede, Z.; Lindquist, S. E. *Sol. Energy Mater. Sol. Cells* **1998**, *51*, 291.
(45) Duffy, N. W.; Peter, L. M.; Wijayantha, K. G. U. *Electrochem. Commun*. **2000**, *2*, 262.
(46) Kruger, J.; Plass, R.; Gratzel, M.; Cameron, P. J.; Peter, L. M. *J. Phys. Chem. B* **2003**, *107*, 7536.
(47) Nusbaumer, H.; Zakeeruddin, S. M.; Moser, J. E.; Gratzel, M. *Chem.—Eur. J.* **2003**, *9*, 3756.
(48) Sapp, S. A.; Elliott, C. M.; Contado, C.; Caramori, S.; Bignozzi, C. A. *J. Am. Chem. Soc.* **2002**, *124*, 11215.
(49) Pelet, S.; Moser, J. E.; Gratzel, M. *J. Phys. Chem. B* **2000**, *104*, 1791.
(50) Hauch, A.; Georg, A. *Electrochim. Acta* **2001**, *46*, 3457.
(51) Desilvestro, J.; Gratzel, M.; Kavan, L.; Moser, J. E.; Augustynski, J. *J. Am. Chem. Soc.* **1985**, *107*, 2988.
(52) Nusbaumer, H.; Moser, J. E.; Zakeeruddin, S. M.; Nazeeruddin, M. K.; Gratzel, M. *J. Phys. Chem. B* **2001**, *105*, 10461.
(53) Bach, U.; Lupo, D.; Comte, P.; Moser, J. E.; Weissortel, F.; Salbeck, J.; Spreitzer, H.; Gratzel, M. *Nature* **1998**, *395*, 583.
(54) Kipling, J. J.; Shooter, P. V. *J. Colloid Interface Sci.* **1966**, *21*, 595.